

NON-ISOTHERMAL INJECTION MOULDING WITH RESIN CURE AND PREFORM DEFORMABILITY

A. FARINA* and L. PREZIOSI**

* *Dipartimento di Matematica "U. Dini"*

Università degli Studi di Firenze

Viale Morgagni 67/a, Firenze, 50135, Italy

`angiolo.farina@math.unifi.it`

** *Dipartimento di Matematica*

Politecnico di Torino

Corso Duca degli Abruzzi 24, Torino, 10129, Italy

`preziosi@polito.it`

Abstract — In this paper a non-isothermal model to simulate some injection moulding processes used to fabricate composite materials is deduced. The model allows the solid constituent in both the dry and the wet region to deform during infiltration. The dry porous material is assumed to behave elastically, while the mixture of resin and preform is assumed to behave as a standard linear solid. The model also takes into account the fact that while infiltrating the liquid undergoes an exothermic cross-linking reaction and eventually gels stopping the infiltration process. Focusing then on one-dimensional problems it is shown that the integration of the mechanical problem in the uninfiltred region can be reduced to the integration of an ordinary differential equation defining either the space independent volume ratio or the location of the infiltration front, depending on whether the flow is driven by a given infiltration velocity or by a given inlet pressure. The remaining system of partial differential equations in the two interfaced and time-dependent domains is then posed with the proper interface and boundary conditions. After writing the problem in a Lagrangian formulation fixed on the solid constituent, domain decomposition techniques are used for the simulation.

Keywords: Composites, Porous media, Injection moulding, Resin transfer moulding (RTM), Analytical modelling.

1. Introduction

Many composite materials are manufactured using industrial processes, usually named RTM (Resin Transfer Molding), SRIM (Structural Resin Injection Molding), SCRIMP (Seeman Composite Resin Infusion Manufacture Process), or squeeze casting, which essentially consist in injecting a metallic, ceramic, or polymeric melt in a porous preform. The solid constituent, which can be for instance made of sponge-like materials, mats, or aligned fibers and is usually called preform, is put in a mold. Then the liquid is introduced through an injection port, while air goes out from suitably located air vents. At the end of the production cycle, the liquid matrix, which should uniformly fill up the whole preform, solidifies holding the reinforcing elements together and enabling the transfer of the major stresses and loads to the solid preform.

In the literature, these processes are modelled assuming that the solid preform does not deform during infiltration. Under this assumption non-isothermal resin injection moulding simulations have been performed for instance by Chan and Hwang (1991, 1992, 1993), by Lin, Lee, and Liou (1991, 1993), and by Young (1994).

On the other hand, non negligible deformations are mentioned or experimentally put in evidence by several authors (Clyne and Mason (1991), Gonzalez-Romero and Macosko (1990), Kim et al. (1991), Lacoste et al. (1991, 1993), Lekakou et al. (1996), Mortensen et al. (1990, 1996), Nam et al. (1995), Rudd et al. (1990, 1992), Yamauchi and Nishida (1995)), and in particular by Lee, Liou and Young's group itself (Han et al. (1993a,b), Trevino et al. (1991), Young et al. (1991).)

In fact, in several practical situations the pressure gradient driving the flow is large enough to significantly compress the reinforcing network. This is particularly evident near the injection port where the liquid matrix entering the mold may push away the preform, forming a fiber-free region. Moreover, infiltration generates a compression in the region near the advancing front which influences the preform permeability.

From an industrial point of view, it is important to have a model which allows to monitor both deformation and stress states in the solid preform. The former in order to quantify the inhomogeneous characteristics of the final products. The latter in order to evaluate in advance the possibility of damages in the reinforcing network, which may lead to material failure.

From these observations, the necessity of including deformations in models aimed at simulating composite materials manufacturing is clear. Keeping this in mind, in previous papers (Preziosi et al. (1996), Ambrosi and Preziosi (1998) and (2000), Billi and Farina (2000)) we have considered the isothermal infiltration problem. In particular, in Preziosi et al. (1996) the uninfilted preform is assumed rigid and the behavior of the system is studied both considering and neglecting inertia and for both an elastic and a Voigt-Kelvin constitutive model for the infiltrated region. Billi and Farina (2000) proved, in the elastic case and under the assumption of negligible inertia, existence and uniqueness of a classical solution and that when the flow is driven by a constant inlet pressure the problem can be put in self-similar form. This, in particular, means that the infiltration front and the sponge border move like the square root of time. In Ambrosi

and Preziosi (1998) the coupled wet/dry problem is studied considering inertia and assuming that both the wet and the dry preform are elastic with the same stress-volume ratio law.

This paper instead deduces a model aimed at simulating non isothermal injection moulding processes, always allowing deformation of the solid preform during the application of the pressure and temperature cycle. In addition, while infiltrating the resin undergoes an exothermic crosslinking chemical reaction, so that it may gel before full infiltration is achieved. Though the chemical reaction could be slowed down by decreasing the temperature, this increases the viscosity of the liquid and therefore slows down the infiltration. From the application viewpoint one has then to find a proper set of parameters leading to a rapid full infiltration with reasonably small compression and without strong inhomogeneities. The model presented in this paper proves to be able to do that.

Besides the region occupied by the liquid only, the infiltration problem presents the formation of two time-dependent domains, one occupied by the solid preform wet by the curing resin, and the other consisting of the uninfiltated solid preform. It is assumed that sharp fronts divide the three domains. If this might be plain for the interface dividing the pure liquid and the wet preform, i.e. one of the borders of the preform, it implies a simplification of capillary phenomena at the interface between the saturated and the dry porous medium. This assumption, often called slug-flow approximation, is reasonable when the applied inlet pressure is much larger than the capillary pressure as occurs in most composite material manufacturing processes. Antonelli and Farina (1999) developed an analysis of such phenomena in a similar framework. The reader is also referred to the papers by Sommer and Mortensen (1996) and Mortensen and Wong (1990) who deal with capillary phenomena in metal matrix composites.

Though the paper specifically refers to the industrial processes mentioned in the beginning, the basic idea can be easily applied to other industrial processes involving infiltration in deformable porous materials, e.g. sponge-like materials.

The paper develops in six sections. After this introduction, the second section presents the three-dimensional non-isothermal model with resin cure. In the third section the solution of the one-dimensional problem in the dry region is addressed. In fact, the mechanical problem can be reduced to the integration of an ordinary differential equation determining either the location of the infiltration front or the volume ratio in the dry region, depending on whether the parameter which is controlled from the outside and which determines the infiltration is the pressure difference between the extrema of the preform or the inflow velocity. The problem then reduces to the integration of the heat equation coupled through the interface conditions to the solution in the infiltrated region. The other interface conditions referring to mechanical state variables rewrite as boundary conditions for the solution in the infiltrated region and depend on how the liquid is pushed in the preform. In the fourth section the coupled initial boundary value problem is posed and written in a Lagrangian formulation. The fifth section briefly describes the numerical method, and discusses the results of some simulations which show how the model can be used to determine the deformation evolution during infiltration and the parameter range for which the preform can be completely infiltrated before resin gels. A final section draws some

conclusions pointing out possible developments.

2. Modelling the Infiltration Problem

Consider an initially dry solid preform, which at time $t = 0$ starts being infiltrated by a resin. Referring to Fig. 1, it is possible to identify two time varying domains, a dry region $\mathcal{D}_d(t)$ and a wet region $\mathcal{D}_w(t)$. If capillarity phenomena are negligible, as occurs in most composite manufacturing processes, which are driven by infiltration pressures much larger than the capillary pressures, the two domains are divided by a sharp infiltration front $\Gamma_i(t)$. Furthermore, we assume that no gas remains entrapped in the wet preform, so that in each domain only two constituents are co-present, the solid and the resin in $\mathcal{D}_w(t)$, and the solid and air in $\mathcal{D}_d(t)$.

Referring to Preziosi (1996) and references therein for further details, we can write for the wet region the following equations

- Conservation of mass of the solid constituent

$$\frac{\partial \phi_s}{\partial t} + \nabla \cdot (\phi_s \mathbf{v}_s) = 0 , \quad (2.1)$$

where \mathbf{v}_s is the velocity of the solid constituent, and ϕ_s is its volume fraction, i.e. the volume occupied by the solid constituent over the total volume;

- Conservation of mass of the liquid constituent

$$\frac{\partial \phi_\ell}{\partial t} + \nabla \cdot (\phi_\ell \mathbf{v}_\ell) = 0 , \quad (2.2)$$

where \mathbf{v}_ℓ is the velocity of the liquid constituent, and ϕ_ℓ is its volume fraction;

- Momentum equation for the mixture

$$\rho_m \left(\frac{\partial \mathbf{v}_m}{\partial t} + \mathbf{v}_m \cdot \nabla \mathbf{v}_m \right) = \nabla \cdot \mathbb{T}_m , \quad (2.3)$$

where \mathbb{T}_m is the stress tensor of the mixture,

$$\rho_m = \rho_s \phi_s + \rho_\ell \phi_\ell , \quad (2.4)$$

is the so-called composite density, i.e. the density of the mixture, while ρ_p is the “true” density of the material which is used as p -constituent and

$$\mathbf{v}_m = \frac{\rho_s \phi_s \mathbf{v}_s + \rho_\ell \phi_\ell \mathbf{v}_\ell}{\rho_m} , \quad (2.5)$$

is the so-called mass average velocity, i.e. the velocity of the center of mass of the mixture.

In the following, the inertial term in (2.3) will be neglected;

- Darcy’s law

$$\phi_\ell (\mathbf{v}_\ell - \mathbf{v}_s) = - \frac{\mathbb{K}(\mathbb{F}_s) \nabla P_\ell}{\mu} , \quad (2.6)$$

where μ is the liquid viscosity, P_ℓ is the pore liquid pressure, and \mathbb{K} is the permeability tensor, which depends on the deformation gradient of the solid constituent \mathbb{F}_s . We recall that if ϕ_* is the volume ratio in the reference configuration, \mathbb{F}_s is linked to the volume ratio by $\det \mathbb{F}_s = \phi_*/\phi_s$. Since we want to consider non-isothermal infiltration processes with resin cure, the viscosity of the resin will depend on its temperature θ , and degree of cure δ_c .

Of course, several corrections can be considered here, e.g. Forchheimer law, or corrections which take into account the non-Newtonian properties of the resin. However, in this paper we proceed assuming the validity of Darcy's model;

- Degree of cure of the resin

$$\frac{\partial \delta_c}{\partial t} + \mathbf{v}_\ell \cdot \nabla \delta_c = f_c(\delta_c, \theta) , \quad (2.7)$$

where f_c is an experimentally determined function describing the chemical reaction. We recall that $\delta_c \in [0, 1]$ as it represents the fraction of cured resin;

- Energy equation for the mixture

$$\rho_m \left(\frac{\partial \varepsilon_m}{\partial t} + \mathbf{v}_m \cdot \nabla \varepsilon_m \right) = \mathbb{T}_m : \nabla \mathbf{v}_m - \nabla \cdot \mathbf{q}_m + \phi_\ell H_c f_c(\delta_c, \theta) , \quad (2.8)$$

where ε_m and \mathbf{q}_m are, respectively, the internal energy and the heat flux related to mixture as a whole, and the last term represents the heat supplied by the exothermic curing reaction of the resin. In particular, H_c is the total heat of reaction.

Equation (2.8) can effectively describe the thermodynamic behavior of the mixture if the resin flow is slow enough, so that the temperature of the bridges and of the pore walls of the preform are allowed to adjust quasistatically to the changes of temperature of the resin flowing through it, so that the two constituents can be always considered in local thermal equilibrium (on the time scale defined by the infiltration velocity) with the same temperature.

Since in resin infiltration problems inertial terms are very small, we will neglect them. In fact, in previous papers (Preziosi et al. (1996) and Ambrosi and Preziosi (1998) and (2000)) which considered inertia, it was noticed that the dimensionless form of the equations presents in front of the inertial term a coefficient which is usually very small in practice. Actually, they showed that inertial terms are important only during the very initial stages of infiltration. In the same papers it has been shown that, under the assumption of elastic constitutive equations, neglecting inertia changes the mathematical structure of the isothermal problem from hyperbolic to parabolic.

Under this hypothesis, Eq.(2.3) rewrites as a stress equilibrium equation

$$\nabla P_\ell = \nabla \cdot \mathbb{T}_m^w , \quad (2.9)$$

if, referring for instance to Terzaghi (1923) and de Boer (1996), one defines the effective stress tensor as

$$\mathbb{T}_m^w \stackrel{\text{def}}{=} \mathbb{T}_m + P_\ell \mathbb{I} . \quad (2.10)$$

Of course, \mathbb{T}_m^w has to be constitutively related to the deformation of the solid constituent with respect to the reference (or natural) configuration and to the fluid properties.

In the following, we will use Darcy's law, the saturation condition $\phi_s + \phi_\ell = 1$, and the stress equilibrium equation to simplify the model (in particular, the energy equation) in a set of equations which results easier to be handled.

The first step is to observe that summing the two continuity equations (2.1, 2.2), one has

$$\nabla \cdot \mathbf{v}_c = 0 , \quad (2.11)$$

where

$$\mathbf{v}_c = \phi_s \mathbf{v}_s + (1 - \phi_s) \mathbf{v}_\ell , \quad (2.12)$$

is the so-called composite velocity.

Using Darcy's law (2.6), Eq.(2.11) can also be written as

$$\nabla \cdot (\mathbf{v}_s + \mathbf{Q}) = 0 , \quad (2.13)$$

where

$$\mathbf{Q} \stackrel{\text{def}}{=} - \frac{\mathbb{K}(\mathbb{F}_s) \nabla P_\ell}{\mu(\delta_c, \theta)} = - \frac{\mathbb{K}(\mathbb{F}_s) \nabla \cdot \mathbb{T}_m^w}{\mu(\delta_c, \theta)} . \quad (2.14)$$

The main characteristic of the model proposed here is to consider the evolution of both the thermal field (and the curing process) and the deformation of the solid preform. To do that one need to pay a particular attention in handling the energy equation. In fact, starting from the ones related to the single constituents and working under the assumption of negligible inertia and unique temperature for the constituents, one can distinguish in the heat flux term \mathbf{q}_m a static part, which can be modelled by Fourier's law with an effective conductivity tensor lk_m , and a dynamic part due to the motion of the constituents, which depends on the diffusive velocities $\mathbf{v}_s - \mathbf{v}_m$ and $\mathbf{v}_\ell - \mathbf{v}_m$

$$\mathbf{q}_m = -lk_m \nabla \theta + \rho_s \phi_s \tilde{C}_s \theta (\mathbf{v}_s - \mathbf{v}_m) + \rho_\ell \phi_\ell \tilde{C}_\ell \theta (\mathbf{v}_\ell - \mathbf{v}_m) - \tilde{\mathbb{T}}_s (\mathbf{v}_s - \mathbf{v}_m) - \tilde{\mathbb{T}}_\ell (\mathbf{v}_\ell - \mathbf{v}_m) \quad (2.15)$$

where \tilde{C}_s and \tilde{C}_ℓ are the heat capacities and $\tilde{\mathbb{T}}_s$ and $\tilde{\mathbb{T}}_\ell$ are the partial stress tensors.

One can then write

$$\begin{aligned} \rho_m C_m \frac{\partial \theta}{\partial t} + [\rho_s \phi_s \tilde{C}_s \mathbf{v}_s + \rho_\ell (1 - \phi_s) \tilde{C}_\ell \mathbf{v}_\ell] \cdot \nabla \theta = \nabla \cdot (\tilde{\mathbb{T}}_s \mathbf{v}_s + \tilde{\mathbb{T}}_\ell \mathbf{v}_\ell) \\ + \nabla \cdot (lk_m \nabla \theta) + (1 - \phi_s) H_c f_c (\delta_c, \theta) , \end{aligned} \quad (2.16)$$

where

$$C_m = \frac{\rho_s \phi_s \tilde{C}_s + \rho_\ell \phi_\ell \tilde{C}_\ell}{\rho_m} , \quad (2.17)$$

and lk_m are, respectively, the heat capacity and conductivity related to the mixture.

In order to further simplify the first term on the right hand side of (2.16), it is useful to recall that the assumptions under which Darcy's law can be obtained from the momentum equation

of the liquid constituent (see Bowen (1980)) imply that the partial stress tensors $\tilde{\mathbb{T}}_s$ and $\tilde{\mathbb{T}}_\ell$ are related to \mathbb{T}_m and P_ℓ through

$$\tilde{\mathbb{T}}_s + \tilde{\mathbb{T}}_\ell = \mathbb{T}_m, \quad \tilde{\mathbb{T}}_\ell = -(1 - \phi_s)P_\ell \mathbb{I}. \quad (2.18)$$

This means that

$$\begin{aligned} \nabla \cdot (\tilde{\mathbb{T}}_s \mathbf{v}_s + \tilde{\mathbb{T}}_\ell \mathbf{v}_\ell) &= \nabla \cdot [-\phi_s P_\ell \mathbf{v}_s - (1 - \phi_s)P_\ell \mathbf{v}_\ell] + \nabla \cdot (\mathbb{T}_m^w \mathbf{v}_s) \\ &= -\nabla \cdot (P_\ell \mathbf{v}_c) + \mathbb{T}_m^w : \nabla \mathbf{v}_s + \mathbf{v}_s \cdot \nabla \cdot \mathbb{T}_m^w, \end{aligned} \quad (2.19)$$

which, using (2.11), (2.9), and (2.6) simplifies to

$$\begin{aligned} \nabla \cdot (\tilde{\mathbb{T}}_s \mathbf{v}_s + \tilde{\mathbb{T}}_\ell \mathbf{v}_\ell) &= -(1 - \phi_s)(\mathbf{v}_\ell - \mathbf{v}_s) \cdot \nabla P_\ell + \mathbb{T}_m^w : \nabla \mathbf{v}_s \\ &= \frac{1}{\mu} \nabla P_\ell \cdot \mathbb{K}(\mathbb{F}_s) \nabla P_\ell + \mathbb{T}_m^w : \nabla \mathbf{v}_s. \end{aligned} \quad (2.20)$$

It is also convenient to rewrite the left hand side of (2.16) so that the material time derivative following the solid constituent appears. This can be obtained observing that

$$\begin{aligned} [\rho_s \phi_s \tilde{C}_s \mathbf{v}_s + \rho_\ell (1 - \phi_s) \tilde{C}_\ell \mathbf{v}_\ell] &= \rho_m C_m \mathbf{v}_s + \rho_\ell \tilde{C}_\ell (1 - \phi_s) (\mathbf{v}_\ell - \mathbf{v}_s) \\ &= \rho_m C_m \mathbf{v}_s + \rho_\ell \tilde{C}_\ell \mathbf{Q}. \end{aligned} \quad (2.21)$$

In conclusion, the heat equation can be written as

$$\begin{aligned} \rho_m C_m \left(\frac{\partial \theta}{\partial t} + \mathbf{v}_s \cdot \nabla \theta \right) &= -\rho_\ell \tilde{C}_\ell \mathbf{Q} \cdot \nabla \theta + \nabla \cdot (k_m \nabla \theta) \\ &\quad + \frac{1}{\mu} \nabla P_\ell \cdot \mathbb{K}(\mathbb{F}_s) \nabla P_\ell + \mathbb{T}_m^w : \nabla \mathbf{v}_s + (1 - \phi_s) H_c f_c(\delta_c, \theta). \end{aligned} \quad (2.22)$$

Finally, using again Darcy's law (2.6) to eliminate the velocity of the liquid constituent the degree of cure equation (2.7) becomes

$$\frac{\partial \delta_c}{\partial t} + \mathbf{v}_s \cdot \nabla \delta_c = -\frac{\mathbf{Q} \cdot \nabla \delta_c}{1 - \phi_s} + f_c(\delta_c, \theta). \quad (2.23)$$

The model in the infiltrated region is then given by Eqs.(2.1), (2.9), (2.13), (2.22), and (2.23), which are in charge of describing the evolution of ϕ_s , \mathbf{v}_s , P_ℓ , θ , and δ_c .

Before proceeding, it is useful to stress the difference between mass average velocity and composite velocity, which is a volume average velocity

$$\mathbf{v}_m = \mathbf{v}_c + \frac{\rho_s - \rho_\ell}{\rho_m} \phi_s (1 - \phi_s) (\mathbf{v}_s - \mathbf{v}_\ell) = \mathbf{v}_c - \frac{\rho_s - \rho_\ell}{\rho_m} \phi_s \mathbf{Q}. \quad (2.24)$$

The following relations will also turn useful

$$\begin{aligned} \rho_m (\mathbf{v}_m - \mathbf{v}_s) &= \rho_\ell (\mathbf{v}_c - \mathbf{v}_s) = -\rho_\ell (1 - \phi_s) (\mathbf{v}_s - \mathbf{v}_\ell) \\ \rho_m (\mathbf{v}_m - \mathbf{v}_\ell) &= \rho_s (\mathbf{v}_c - \mathbf{v}_\ell) = \rho_s \phi_s (\mathbf{v}_s - \mathbf{v}_\ell). \end{aligned} \quad (2.25)$$

One can proceed in a similar way to obtain the system of evolution equations valid in the dry region with the simplifications due to the fact that air density and viscosity are very small.

Therefore, it is easily expelled from the dry preform, and its contribution to the stress of the mixture \mathbb{T}_m^d and to the inertial term can be neglected. Hence, the momentum equation does not involve any contribution from the gas. Actually, one can forget about mass and momentum balance for the gas, and coherently assume that its pressure in the dry region is constant and $\mathbb{T}_m^d = \mathbb{T}_s$. Moreover, the mass average velocity is equal to the velocity of the solid constituent, the composite density is given by $\rho_m = \rho_s \phi_s$, and, the composite velocity by $\mathbf{v}_c = \phi_s \mathbf{v}_s + (1 - \phi_s) \mathbf{v}_{\text{air}}$.

Similarly, considering the smallness of its heat capacity and conductivity, also in the energy equation there is no contribution from the gas. Therefore, in the dry region the heat capacity and the heat conductivity of the mixture are simply $\rho_m C_m^d = \rho_s \phi_s \tilde{C}_s$ and $\mathbb{k}_m^d = \phi_s \mathbb{k}_s$, where \mathbb{k}_s is the heat conductivity of the solid constituent.

Of course, a further simplification is due to the fact that in the dry region there is no reaction, since no resin is present.

One then has

$$\left\{ \begin{array}{l} \frac{\partial \phi_s}{\partial t} + \nabla \cdot (\phi_s \mathbf{v}_s) = 0 , \\ \nabla \cdot \mathbb{T}_m^d = \mathbf{0} , \\ \rho_s \phi_s \tilde{C}_s \left(\frac{\partial \theta}{\partial t} + \mathbf{v}_s \cdot \nabla \theta \right) = \mathbb{T}_m^d : \nabla \mathbf{v}_s + \nabla \cdot (\phi_s \mathbb{k}_s \nabla \theta) , \end{array} \right. \quad \text{in } \mathcal{D}_d(t) \quad (2.26)$$

Equations (2.9), (2.13), (2.22), (2.23) and (2.26) still need the identification of μ , f_c , \mathbb{K} , \mathbb{k}_m , \tilde{C}_s , \tilde{C}_ℓ , and of the constitutive equations for the stress tensors. In this paper \tilde{C}_s and \tilde{C}_ℓ will be assumed to be constant, and \mathbb{k}_m to be given by

$$\mathbb{k}_m = \phi_s \mathbb{k}_s + (1 - \phi_s) \mathbb{k}_\ell , \quad (2.27)$$

where \mathbb{k}_ℓ is the heat conductivity of the liquid (see Markov and Preziosi (1999)).

Several models have been proposed for the remaining parameters (see Preziosi (1996) for a review). In order to use the experimental results by Young et al. (1991) and Sommer and Mortensen (1996), the simulation to follow will take

$$\mu(\delta_c, \theta) = \begin{cases} \bar{\mu} e^{E_\mu / \mathcal{R}\theta} \left(\frac{\delta_g}{\delta_g - \delta_c} \right)^{c_\mu + d_\mu \delta_c} & \text{if } \delta_c < \delta_g \\ \infty & \text{otherwise} \end{cases} \quad (2.28)$$

where δ_g is the resin gel conversion, E_μ is the activation energy, \mathcal{R} is gas constant, and $\bar{\mu}$, c_μ , and d_μ are constant,

$$K_{ij}(\mathbb{F}_s) = \bar{K}_i e^{-n_i \phi_s} \delta_{ij} , \quad (2.29)$$

where δ_{ij} is the Kronecker delta, and \bar{K}_i and n_i are constant, and Kamal and Sorour's (1973) model

$$f_c(\delta_c, \theta) = \left[c_1 \exp\left(-\frac{E_1}{\mathcal{R}\theta}\right) + c_2 \exp\left(-\frac{E_2}{\mathcal{R}\theta}\right) \delta_c^{m_c} \right] (1 - \delta_c)^{n_c} , \quad (2.30)$$

where m_c and n_c describe the order of reaction, c_1 and c_2 are the reaction rate constants, and E_1 and E_2 are again activation energies.

In addition, continuum mechanics concepts can help formulating the constitutive equation for the stress tensors \mathbb{T}_s and \mathbb{T}_m^w , which can be, in principle, validated directly, through suitable experiments.

Unfortunately, there are only very few results oriented at describing the viscoelastic behaviour of wet and dry preforms. Kim et al. (1991) performed some experiments to study the stress relaxation properties of a wet preform and found a spectrum of relaxation times. They also pointed out the different behavior of wet and dry preform subject to static compression. Nam et al. (1995) investigated creep deformation of a commercial prepreg, measuring a retardation time of the order of 200 seconds. In addition, several other authors (Han et al. (1993a,b), Lekakou et al. (1996), Sommer and Mortensen (1996), Reboredo and Rojas (1988), and Trevino et al. (1991)) have noticed a viscoelastic behavior of the materials they use with non negligible relaxation or retardation times.

In agreement with the just mentioned experimental results and the qualitative argument that in the wet porous materials the solid and the liquid constituents cannot deform independently but have to carry the load by joint deformation, in this paper we assume that the dry and wet material behave respectively like an elastic and a standard linear solid.

As far as the jump conditions are concerned, one can start observing that the border of the preform near the inlet and the infiltration front are material surfaces of discontinuity fixed on the solid and liquid constituent, respectively. Under the hypothesis used in this paper, following Müller (1975) and Liu (1980) one can then derive the following interface conditions related to mass, momentum and energy balance

$$[[\mathbf{v}_c]] \cdot \mathbf{n} = 0 \ , \quad (2.31)$$

$$[[\mathbb{T}_m]] \mathbf{n} = \mathbf{0} \ , \quad (2.32)$$

$$[[\varepsilon_m]] \rho_m (\mathbf{v}_m - \mathbf{v}_\sigma) \cdot \mathbf{n} - [[\mathbf{v}_m \cdot (\mathbb{T}_m \mathbf{n})]] + [[\mathbf{q}_m]] \cdot \mathbf{n} = 0 \ , \quad (2.33)$$

where \mathbf{n} is the normal to the surface of discontinuity, \mathbf{v}_σ its velocity, and $[[\mathbf{f}]]$ denotes the jump of \mathbf{f} across it.

Furthermore, as usual, we shall assume

$$[[\theta]] = 0 \ . \quad (2.34)$$

Equation (2.31) is classical, and Eq.(2.32) is compatible with the fact that inertial terms have been neglected in the momentum equation. For the same reason, the term $\frac{1}{2} \rho_m v_m^2 (\mathbf{v}_m - \mathbf{v}_\sigma) \cdot \mathbf{n}$ does not appear in (2.33). Actually, using (2.15), the hypothesis on the stresses, (2.24), (2.25), and (2.32), Eq.(2.33) can be rewritten as

$$[[k_m \nabla \theta]] \cdot \mathbf{n} + [[\mathbf{v}_s]] \cdot (\mathbb{T}_m^w \mathbf{n}) = [[\rho_s \phi_s \tilde{C}_s (\mathbf{v}_s - \mathbf{v}_\sigma) \cdot \mathbf{n}]] + [[\rho_\ell (1 - \phi_s) \tilde{C}_\ell (\mathbf{v}_\ell - \mathbf{v}_\sigma) \cdot \mathbf{n}]] \ . \quad (2.35)$$

If the material interface is fixed on the liquid constituent and \tilde{C}_s is assumed continuous across it, then the right hand side of (2.35) vanishes. The same is analogously true if the

material interface is fixed on the solid constituent and \tilde{C}_ℓ is assumed continuous across it. Using (2.31) and (2.32) we can then write

$$[[Ik_m \nabla \theta]] \cdot \mathbf{n} + [[\mathbf{v}_s]] \cdot (\mathbb{T}_m^w \mathbf{n}) = 0 . \quad (2.36)$$

3. The One-Dimensional Problem in the Uninfiltrated Region

Consider, now, the one-dimensional infiltration problem along a principal direction of the preform permeability tensor, and, referring to Fig. 2, denote by $x_f(t)$ the left border of the preform and by $x_i(t)$ the infiltration front. A fully draining boundary constrains the right border of the solid preform to be fixed at $x = L$, but allows, at the same time, both air and liquid matrix to pass through with no resistance.

For $t < 0$ the whole preform is dry, at rest, and compressed at a given volume ratio , i.e.

$$\begin{cases} \phi_s(x, t < 0) = \Psi_0 & \text{for } x \in [0, L]; \\ x_f(t < 0) = x_i(t < 0) = 0 . \end{cases} \quad (3.1)$$

The liquid matrix flows in the positive direction either pushed at a given inflow velocity, or forced by a pressure gradient and at $t = 0$ it touches the left border of the preform. As shown in Fig. 2, the incoming liquid then compresses the porous material while the fluid starts infiltrating. In particular, as will be shown at the end of this section, if the flow is pressure driven, inertia is neglected and on the dry preform an effective elasticity assumption is made, the preform instantaneously compresses as it is touched by the fluid to balance the applied pressure. Of course, these assumptions are a strong approximation as creep phenomena and plastic deformation, e.g. due to fiber displacement in fiber reinforced materials, usually occur, and inertial effects become important at the beginning of pressure driven infiltration (see, Ambrosi and Preziosi (1998) and (2000)).

Therefore, while the right border of the porous solid stays fixed at $x = L$, the other one moves to $x = x_f(t)$, and part of the preform, precisely up to $x = x_i(t)$, wets up. The wet and dry regions are then defined by $\mathcal{D}_w(t) = (x_f(t), x_i(t))$ and $\mathcal{D}_d(t) = (x_i(t), L)$, respectively.

As infiltration proceeds both the dry and the wet preform compress or expand back, according to the flow conditions. However, still assuming that no plastic phenomena occur, the undeformed configuration can be reached again only if liquid inflow is stopped and further relaxation is allowed.

Before proceeding, it is then useful to observe that, in one-dimensional problems, the condition that \mathbf{v}_c is divergence-free rewrites

$$\frac{\partial v_c}{\partial x} = 0 , \quad \text{in } \mathcal{D}_w(t) \cup \mathcal{D}_d(t) , \quad (3.2)$$

which implies that the composite velocity is space independent in each sub-domain

$$v_c(x, t) = \begin{cases} v_c^w(t) & \text{in } \mathcal{D}_w(t) ; \\ v_c^d(t) & \text{in } \mathcal{D}_d(t) . \end{cases} \quad (3.3)$$

Since, according to (2.31), v_c is also continuous across the material interfaces $x_f(t)$ and $x_i(t)$, then, going all the way down where there is resin only, one has that the composite velocity has to be constantly equal to the inflow velocity

$$v_c(x, t) = u_{\text{in}}(t) \quad \forall x \in \mathcal{D}_w(t) \cup \mathcal{D}_d(t) . \quad (3.4)$$

The above relation and Darcy's law allow to determine the velocity of the constituents and the mass average velocity in the wet region as

$$v_s = u_{\text{in}} - Q , \quad (3.5)$$

$$v_\ell = u_{\text{in}} + \frac{\phi_s}{1 - \phi_s} Q , \quad \text{in } \mathcal{D}_w(t) \quad (3.6)$$

$$v_m = u_{\text{in}} - \frac{\rho_s - \rho_\ell}{\rho_m} \phi_s Q , \quad (3.7)$$

where Q is given by

$$Q = - \frac{K(\phi_s)}{\mu} \frac{\partial \tau_m}{\partial x} , \quad (3.8)$$

and τ_m denotes the xx -component of \mathbb{T}_m^w . Equations (3.5) and (3.6) will turn useful in simplifying the modeling as well as in determining the evolution equations for the free boundaries $x_f(t)$ and $x_i(t)$, which are material surfaces for the solid and the liquid, respectively.

In one-dimensional problems, saying that the stress depends only on the strain is equivalent to saying that it depends on the volume ratio as the only non vanishing component of the strain tensor can be one-to-one related to ϕ_s . Therefore, focusing on the dry region and denoting by τ_s the xx -component of \mathbb{T}_s ,

$$\tau_s = -\Sigma_s(\phi_s) , \quad \text{for } x \in (x_i(t), L) . \quad (3.9)$$

Equation (3.9) together with the stress equilibrium equation $\partial \tau_s / \partial x = 0$ implies that the volume ratio in the dry region is space-independent, that is

$$\phi_s(x, t) = \Psi(t) , \quad \text{for } x \in (x_i(t), L) . \quad (3.10)$$

Therefore, from the continuity equation and the fact that the preform is constrained by a fixed draining boundary at $x = L$ (that is, its velocity vanishes there), one has

$$v_s(x, t) = \frac{\Psi'(t)}{\Psi(t)}(L - x) , \quad \text{for } x \in (x_i(t), L) , \quad (3.11)$$

where $\Psi' = d\Psi/dt$. From now on primes will denote differentiation with respect to time.

The determination of $\Psi(t)$ is strongly related to the method used to inject the resin in the solid preform or, more properly, to the parameter which is controlled during injection. In fact, infiltration can be achieved either as a result of resin injection at a given inflow velocity u_{in} , or as a result of a given inlet pressure $\Delta P(t)$.

The starting point which can be used to link u_{in} or ΔP to the volume ratio in the dry region $\Psi(t)$ is to use (3.10) and (3.11) in the chain of equalities obtained evaluating the composite velocity, which from (3.4) is always equal to the inflow velocity, on both sides of $x_i(t)$

$$\phi_s v_s + (1 - \phi_s) v_\ell = \Psi'(L - x_i) + (1 - \Psi) v_\ell = u_{\text{in}} , \quad \text{on } x_i(t) . \quad (3.12)$$

Recalling (3.5) and the fact that $x_i(t)$ is a material interface fixed on the liquid phase

$$x_i'(t) = v_\ell(x_i(t), t) , \quad (3.13)$$

one can write

$$\phi_s(u_{\text{in}} - Q) + (1 - \phi_s)x_i' = -[(1 - \Psi)(L - x_i)]' = u_{\text{in}} . \quad (3.14)$$

3.1 Velocity Driven Infiltration

If $u_{\text{in}}(t)$ is a given function of time, e.g. u_{in} constant, from (3.14) the evolution of the volume ratio in the dry region $\Psi(t)$ is determined by the initial value problem

$$\begin{cases} [(1 - \Psi)(L - x_i)]' = -u_{\text{in}}(t) , \\ \Psi(0) = \Psi_0 , \end{cases} \quad (3.15)$$

where Ψ_0 is the initial compression of the sponge.

The integration of (3.15) can be actually performed to give

$$\Psi(t) = \frac{1}{L - x_i(t)} \left[\int_0^t u_{\text{in}}(s) ds - x_i(t) + \Psi_0 L \right] , \quad (3.16)$$

where $x_i(t)$ is determined integrating Eq.(3.13), which using (3.6) rewrites

$$\begin{cases} x_i' = u_{\text{in}}(t) + \left(\frac{\phi_s}{1 - \phi_s} Q \right) (x_i(t^-), t) \\ x_i(0) = 0 . \end{cases} \quad (3.17)$$

Of course, the term in bracket is evaluated coming to the infiltration front from the wet region. The free boundary problem is then characterized by a non standard boundary condition on $x_i(t)$ for the volume ratio, since it is linked to Ψ through (3.16), which depends on $x_i(t)$. In turn, $x_i(t)$ is determined by the solution of the system of partial differential equations through (3.17) starting from the initial condition $x_i(0) = 0$.

3.2 Pressure Driven Infiltration

If, instead, the inlet pressure $\Delta P(t)$ is given, then since inertia has been neglected, one can integrate the momentum equations. The continuity of stress across the interfaces x_f and x_i then states that the applied pressure drop is equal to the stress in the dry solid

$$\tau_s(x, t) = -\Delta P(t) , \quad \text{for } x \in (x_i(t), L) \quad \text{and } t > 0 , \quad (3.18)$$

and, therefore, from (3.9) and (3.10)

$$\Psi(t) = \Sigma_s^{-1}(\Delta P(t)) , \quad \text{for } t > 0 , \quad (3.19)$$

where Σ_s^{-1} is the inverse of the stress-volume ratio relation in (3.9).

It should be noted that due to the elasticity of the dry preform, the application of the inlet pressure generates a immediate compression of the preform from the initial location $x_i(t = 0^-) = x_f(t = 0^-) = 0$. Using the conservation of mass of the solid constituent this can be quantified as

$$\Psi(t = 0^+)(L - x_i(t = 0^+)) = \Psi_0 L , \quad (3.20)$$

where $\Psi(t = 0^+) = \Sigma_s^{-1}(\Delta P(0))$.

In the following we will assume that $\Psi_0 \leq \Psi(t = 0^+)$, which determines

$$x_i(t = 0^+) = L \left(1 - \frac{\Psi_0}{\Sigma_s^{-1}(\Delta P(0))} \right) > 0 . \quad (3.21)$$

The case $\Psi_0 > \Psi(t = 0^+)$ corresponds to a strong pre-compression of the preform with a mold pressure higher then the infiltration pressure. In this case, $x_i(t = 0^+) = 0$, because it can not move to negative values of x for the presence of the mold. In particular, if it is possible to pre-compress the preform pressing the mold with a pressure equal to the infiltration pressure, i.e. $\Sigma_s(\Psi_0) = \Delta P$, then the infiltration of the resin would not produce the initial movement of the preform expressed by (3.21).

The velocity of the solid constituent is again given by (3.11). In particular, if the applied inlet pressure is constant in time, then from (3.19) the void ratio is constant in time and the velocity vanishes. This effect was noticed, for instance, by Sommer and Mortensen (1996) who, on the basis of their experimental observations, assumed in their analysis that the dry part does not move until the infiltration front wets the material. Of course, this is not related to any rigidity assumption on the dry material, but it is just that in it the volume ratio is so that the stress constantly balances the constant applied pressure and therefore it does not change.

The evolution equation determining $x_i(t)$ can be obtained eliminating $u_{in}(t)$ from (3.14) and using (3.13) and (3.6). This gives

$$[(1 - \Psi)(L - x_i)]' + x_i'(t) = \left(\frac{\phi_s Q}{1 - \phi_s} \right) (x_i(t), t) , \quad (3.22)$$

which, linked to (3.21) gives the initial value problem determining the evolution of the interface

$$\begin{cases} (\Psi x_i)' = L\Psi' + \left(\frac{\phi_s Q}{1 - \phi_s} \right) (x_i(t), t) , \\ x_i(0) = L \left(1 - \frac{\Psi_0}{\Sigma_s^{-1}(\Delta P(0))} \right) . \end{cases} \quad (3.23)$$

Actually, Eq.(3.23) could be integrated to give

$$x_i(t) = L \left[1 - \frac{\Psi_0}{\Psi(t)} \right] + \frac{1}{\Psi(t)} \int_0^t \frac{\phi_s(x_i(s), s)}{1 - \phi_s(x_i(s), s)} Q(x_i(s), s) ds , \quad (3.24)$$

or

$$\Psi(t)x_i(t) = L(\Psi(t) - \Psi_0) + \int_0^t \frac{\phi_s(x_i(s), s)}{1 - \phi_s(x_i(s), s)} Q(x_i(s), s) ds . \quad (3.25)$$

The inflow velocity is then determined by differentiating (3.25) and substituting the result in (3.14)

$$u_{\text{in}}(t) = (L - x_i(t)) \frac{\Psi'(t)}{\Psi(t)} + \left[\frac{1}{\Psi(t)} - 1 \right] \left(\frac{\phi_s Q}{1 - \phi_s} \right) (x_i(t), t) . \quad (3.26)$$

In conclusion, while in the case of a velocity driven infiltration $u_{\text{in}}(t)$ is given and one has $\Psi(t)$ explicitly given in terms of $x_i(t)$, which is determined by solving the Cauchy problem (3.17), the application of a pressure readily determines $\Psi(t)$ through (3.19). One then has to determine the inflow velocity $u_{\text{in}}(t)$, or, equivalently, $x_i(t)$ through the Cauchy problem (3.23).

However, in both cases the solution in the dry domain is intimately coupled to the one in the wet domain, even in the simpler isothermal case.

It can be also remarked that while the solution related to a constant inlet pressure in general presents for ϕ_s a discontinuity at time $t = 0$, the solution related to a given inflow velocity presents only a discontinuity in slope at time $t = 0$.

4. The Coupled Infiltration Problems

In Section 3, we have partially solved the mechanical problem relating the space independent evolution of the volume ratio to the dynamics of the infiltration front.

The solution of the system (2.26) is completed by integrating the heat equation, which using (3.10) and (3.11) simplifies to

$$\rho_s C_s \left[\Psi(t) \frac{\partial \theta}{\partial t} + \Psi'(t) (L - x) \frac{\partial \theta}{\partial x} \right] = \frac{\Psi'(t)}{\Psi(t)} \Sigma_s(\Psi(t)) + \Psi \frac{\partial}{\partial x} \left(k_s \frac{\partial \theta}{\partial x} \right) \quad \text{in } \mathcal{D}_d(t) . \quad (4.1)$$

It need be mentioned that in one-dimensional problems the dependence of the parameters on the deformation gradient is equivalent to a dependence on the volume ratio, which is directly related to the determinant of \mathbb{F}_s (see Eq.(4.8)).

Of course, the solution is coupled with the one in the wet region $\mathcal{D}_w(t)$, which in one dimension can be simplified to

$$\left\{ \begin{array}{l} \frac{\partial \phi_s}{\partial t} + u_{\text{in}}(t) \frac{\partial \phi_s}{\partial x} = \frac{\partial}{\partial x} (\phi_s Q) , \\ \rho_m C_m \left(\frac{\partial \theta}{\partial t} + v_s \frac{\partial \theta}{\partial x} \right) = -\rho_t \tilde{C}_t Q \frac{\partial \theta}{\partial x} - \frac{\partial}{\partial x} (Q \tau_m) \\ \quad + \frac{\partial}{\partial x} \left(k_m \frac{\partial \theta}{\partial x} \right) + (1 - \phi_s) H_c f_c(\delta_c, \theta) , \\ \frac{\partial \delta_c}{\partial t} + v_s \frac{\partial \delta_c}{\partial x} = -\frac{Q}{1 - \phi_s} \frac{\partial \delta_c}{\partial x} + f_c(\delta_c, \theta) , \end{array} \right. \quad \text{in } \mathcal{D}_w(t) \quad (4.2)$$

where Q is defined in (3.8) and, as already discussed in Section 2, it is assumed that the wet preform behaves like a standard linear solid. However, as at equilibrium the stress is usually

related to the strain ϵ by a nonlinear relation, the constitutive law is modified to

$$\lambda \left(\frac{\partial \tau_m}{\partial t} + v_s \frac{\partial \tau_m}{\partial x} - 2a \tau_m \frac{\partial v_s}{\partial x} \right) + \tau_m = \text{with } \Lambda > \lambda \quad (4.3)$$

$$- \Lambda \left[\left(\frac{\partial \tilde{\Sigma}(\epsilon)}{\partial t} + v_s \frac{\partial \tilde{\Sigma}(\epsilon)}{\partial x} \right) - 2a \tilde{\Sigma}(\epsilon) \frac{\partial v_s}{\partial x} \right] - \tilde{\Sigma}(\epsilon)$$

where the function $\tilde{\Sigma}(\epsilon)$ can be determined by static stress-strain measurement, and the characteristic times λ and Λ , usually called relaxation and retardation times respectively, can be evaluated by stress relaxation and creep tests (see, for instance, Malvern (1969) and Joseph(1990).) The parameter a appearing in (4.3) ranges between $[-1, 1]$ and determines the type of invariant derivative. In particular, $a = 1, 0, -1$ correspond respectively to the so-called upper convected, corotational, and lower convected invariant derivative. It should be mentioned that in (4.3) we implicitly assumed that the velocity appearing in the invariant derivative is the one related to the solid. This choice is based on the type of boundary conditions required by Eq.(4.3) and by the other candidates obtained replacing v_s with other velocities, say v_m or v_c . However, the problem of which is the correct velocity to be used in the constitutive equation is still an open question which should be analyzed also on the basis of experimental results.

The introduction of

$$S_m = \lambda \tau_m + \Lambda \tilde{\Sigma}(\epsilon) , \quad (4.4)$$

simplify Eq.(4.3) to

$$\frac{\partial S_m}{\partial t} + v_s \frac{\partial S_m}{\partial x} - 2a S_m \frac{\partial v_s}{\partial x} + \frac{S_m}{\lambda} = \left(\frac{\Lambda}{\lambda} - 1 \right) \tilde{\Sigma}(\epsilon) . \quad (4.5)$$

It can be readily realized that if $\lambda = \Lambda$, then Eq.(4.5) joined with suitable initial and boundary conditions allows the solution

$$S_m = 0 \quad \text{or} \quad \tau_m = -\tilde{\Sigma}(\epsilon) , \quad (4.6)$$

i.e. the material behaves elastically. In continuum mechanics this is a well known property of the constitutive models corresponding to standard linear solids.

It should be noticed that in one-dimensional problems the strain ϵ is related to the volume ratio through

$$\epsilon = \frac{1}{2} \left(\frac{\Psi_0^2}{\phi_s^2} - 1 \right) . \quad (4.7)$$

Therefore, one can define

$$\Sigma(\phi_s) = \tilde{\Sigma} \left(\frac{1}{2} \left(\frac{\Psi_0^2}{\phi_s^2} - 1 \right) \right) .$$

From a computational point of view it is convenient to formulate the problem in a Lagrangian framework, introducing the coordinate ξ fixed on the solid constituent. Recalling that

$$\frac{\partial x}{\partial \xi} = \det \mathbb{F}_s = \frac{\Psi_0}{\phi_s} , \quad (4.8)$$

and Eqs.(3.5), one then has

$$\left\{ \begin{array}{l} \frac{d_s \phi_s}{dt} = \frac{\phi_s^2}{\Psi_0} \frac{\partial}{\partial \xi} \left(\widehat{Q} \frac{\partial \tau_m}{\partial \xi} \right) , \\ \rho_m C_m \frac{d_s \theta}{dt} = \frac{\phi_s}{\Psi_0} \left[-\rho_\ell \widetilde{C}_\ell \widehat{Q} \frac{\partial \tau_m}{\partial \xi} \frac{\partial \theta}{\partial \xi} - \frac{\partial}{\partial \xi} \left(\tau_m \widehat{Q} \frac{\partial \tau_m}{\partial \xi} \right) \right. \\ \quad \left. + \frac{\partial}{\partial \xi} \left(k_m \frac{\phi_s}{\Psi_0} \frac{\partial \theta}{\partial \xi} \right) \right] + (1 - \phi_s) H_c f_c(\delta_c, \theta) , \\ \frac{d_s \delta_c}{dt} = -\frac{\widehat{Q}}{1 - \phi_s} \frac{\phi_s}{\Psi_0} \frac{\partial \tau_m}{\partial \xi} \frac{\partial \delta_c}{\partial \xi} + f_c(\delta_c, \theta) , \\ \frac{d_s S_m}{dt} = -\frac{S_m}{\lambda} + \left(\frac{\Lambda}{\lambda} - 1 \right) \Sigma(\phi_s) - 2a \frac{\phi_s}{\Psi_0} S_m \frac{\partial}{\partial \xi} \left(\widehat{Q} \frac{\partial \tau_m}{\partial \xi} \right) , \end{array} \right. \quad \text{in } \mathcal{D}_w(t) \quad (4.9)$$

and

$$\rho_s C_s \Psi(t) \frac{d_s \theta}{dt} = \frac{\Psi'(t)}{\Psi(t)} \Sigma_s(\Psi(t)) + \frac{\Psi^3(t)}{\Psi_0^2} \frac{\partial}{\partial \xi} \left(k_s \frac{\partial \theta}{\partial \xi} \right) \quad \text{in } \mathcal{D}_d(t) , \quad (4.10)$$

where

$$\tau_m = \frac{S_m}{\lambda} - \frac{\Lambda}{\lambda} \Sigma(\phi_s) , \quad (4.11)$$

$$\widehat{Q} = \begin{cases} -\frac{K(\phi_s)}{\mu(\delta_c, \theta)} \frac{\phi_s}{\Psi_0} & \text{if } \delta_c < \delta_g ; \\ 0 & \text{if } \delta_c \geq \delta_g , \end{cases} \quad (4.12)$$

and

$$\frac{d_s(\cdot)}{dt} = \frac{\partial(\cdot)}{\partial t} + v_s \frac{\partial(\cdot)}{\partial x} \quad (4.13)$$

denotes the derivative following the solid constituent. In the simulation to follow we will choose a corotational derivative, i.e. $a = 0$.

In order to solve the systems of equations (4.8)–(4.9) we still need to determine the evolution equations describing the movement of the interface $x_i(t)$ relative to the solid, which is given by Darcy's law evaluated at the infiltration front (see also (3.13))

$$\xi_i' = \left(\frac{\phi_s}{\Psi_0} \frac{Q}{1 - \phi_s} \right) (\xi_i(t), t) , \quad (4.14)$$

where $\xi_i(t)$ denotes the location of the infiltration front in the reference configuration. Of course, in a Lagrangian framework the free border $x_f(t)$, which is a material interface fixed on the solid constituent, is fixed at $\xi = 0$. Recalling (3.5), its position in the laboratory frame can be computed integrating

$$x_f' = u_{\text{in}}(t) - Q(x_f(t), t) . \quad (4.15)$$

As far as the interface and boundary conditions are concerned, at the preform boundary $\xi = \xi_f = 0$, Eqs.(2.32) and (2.34) rewrite

$$\tau_m(\xi = 0, t) = 0 , \quad (4.16)$$

$$\theta(\xi = 0, t) = \theta_{\text{in}}(t) . \quad (4.17)$$

Furthermore, since in our problem $v_\ell(x_f(t), t) > v_s(x_f(t), t) = x'_f(t)$, and $v_\ell(x_i(t), t) = x'_i(t)$, the characteristics related to the hyperbolic resin conversion equation enter the domain through $x_f(t)$ whenever $Q(x_f(t), t) > 0$. Therefore, we obviously need provide the inflow cure state in $x_f(t)$

$$\delta_c(\xi = 0, t) = \delta_{\text{in}}(t) . \quad (4.18)$$

At the infiltration front $\xi_i(t)$, Eqs.(2.32), (2.34), and (2.36) specialize respectively to

$$\tau_m = -\Sigma_s(\Psi(t)) , \quad (4.19)$$

$$\theta^w = \theta^d , \quad \text{on } \xi_i(t) \quad (4.20)$$

$$k_m \frac{\phi_s}{\Psi_0} \frac{\partial \theta^w}{\partial \xi} = k_s \frac{\Psi(t)}{\Psi_0} \frac{\partial \theta^d}{\partial \xi} - \left(1 - \frac{\phi_s}{\Psi(t)}\right) \frac{\hat{Q}}{1 - \phi_s} \frac{\partial \tau_m}{\partial \xi} \Sigma_s(\Psi(t)) , \quad (4.21)$$

where Eqs.(3.5), (3.6) and (2.31) evaluated at the infiltration front have been used and θ_w and θ_d are the temperatures in the wet and in the dry regions, respectively.

Finally, at $\xi = L$ the condition

$$\theta(L, t) = \theta_L(t) , \quad (4.22)$$

has to be provided.

In addition the hyperbolic constitutive equation (4.5) needs other boundary conditions where the characteristics related to the convective velocity enter the domain \mathcal{D}_w . The border $x_f(t)$ is fixed on the solid, and therefore a characteristic runs along it. On the other hand, at $x_i(t)$ the infiltration front is wetting more and more solid, i.e. $v_\ell > v_s$ as implied by (2.6). Therefore an additional condition has to be given on it, i.e. on $\xi_i(t)$.

Before tackling the question of determining which boundary condition should be imposed, we observe that if the wet and dry material respond elastically but according to different stress-strain relations, then the continuity of stress across the infiltration front implies that the volume ratio is discontinuous, adjusting in response of the different stress-volume ratio relationships (see Fig. 3). This means that the region around a material point of the dry region is compressed at a volume ratio Ψ corresponding to a stress $\tau_s = -\Sigma_s(\Psi)$, till it is wet by the infiltration front. At this point due to the continuity of stress across x_i its stress is still $\tau_m = \tau_s = -\Sigma_s(\Psi)$, but since $\tau_m = -\Sigma(\phi_s)$ with $\Sigma < \Sigma_s$, the region suddenly compresses to a higher volume ratio $\phi_s = \Sigma^{-1}(\Sigma_s(\Psi)) > \Psi$, as can be understood following the arrowed line in Fig. 4. This immediate response is a general characteristic of elastic materials, which has been put in evidence in the framework of wetting deformable porous media in Farina and Preziosi (1999).

As a consequence, since the composite velocity is continuous and the volume ratio is not, the velocity of the solid constituent is discontinuous. This would be a direct consequence of the elasticity assumption with different stress-strain relations in the two regions, which, however, we are not claiming to be the exact choice. As explained above, when wet by the infiltration front, the material immediately compresses to achieve instantaneously the same value of stress on both sides of the infiltration front causing the discontinuity in velocity.

If, instead, the material exhibits creep phenomena (e.g., for Voigt-Kelvin or standard linear solids), then the volume ratio of the point considered above will take some time to adjust to the difference of constitutive equation as the infiltration front is passed by. Following this argument, with the help of Fig. 4, one can then realize that besides the stress also the volume ratio should be continuous across the infiltration front

$$\phi_s(\xi_i(t), t) = \Psi(t) , \quad (4.23)$$

which also implies the continuity of v_s and of heat flux

$$k_m \frac{\partial \theta_w}{\partial \xi}(\xi_i(t), t) = k_s \frac{\partial \theta_d}{\partial \xi}(\xi_i(t), t) . \quad (4.24)$$

In terms of S_m Eqs.(4.16), (4.19), and (4.23) imply that

$$S_m(\xi_i(t), t) = \Lambda \Sigma(\Psi(t)) - \lambda \Sigma_s(\Psi(t)) \quad (4.25)$$

$$\phi(\xi_f, t) = \Sigma^{-1} \left(\frac{S_m(\xi_f, t)}{\Lambda} \right) \quad (4.26)$$

Finally, it need be mentioned that the assumption of negligible pressure drop in the dry preform together with the assumption of negligible inertia leads to an initial discontinuity in stress for the pressure driven problem since it vanishes at the preform border and is equal to the pressure drop at the infiltration front and the two interfaces coincide at time $t = 0$.

5. Numerical Results

In this section we will present the results of some simulation of pressure driven flow. The free boundary value problem (4.9), (4.10), (4.14), (4.17), (4.18), (4.20), (4.22)–(4.26) is integrated using an implicit finite difference method, in which the time step is chosen so that the infiltration front ξ_i jumps from node to node. This is achieved integrating

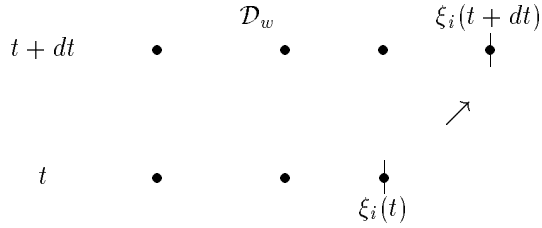
$$\frac{dt}{d\xi_i} = \frac{1 - \phi_s}{Q}(\xi_i, t(\xi_i)) , \quad (5.1)$$

rather than (4.14).

This has also the advantage of setting smaller time steps when the infiltration velocity is higher and the dynamics is evolving more rapidly and larger time steps when infiltration is slowing down. However, as infiltration does not stop exactly at a discretization node and one has to evaluate the time step needed to reach the next discretization node, some accuracy is lost when gelling is about to occur. After gelling has put an end to the infiltration process, the time step is fixed according to accuracy requirements.

To be more specific a backward Euler method has been used, since the more accurate Crank-Nicholson method suffers from the need of obtaining in the wet region the value of the derivatives

of some variables at the advancing infiltration front at time t , which can not be done by central differences, as shown in the stencil below



A Crank-Nicholson method has been instead used after infiltration stops.

As far as the integration of the hyperbolic degree of cure equation is concerned, an implicit upwind method is used for the central nodes. The infiltration front, instead, follows the characteristic of the equation and then the degree of cure there is obtained by direct integration along the characteristic.

An implicit upwind method is again used for the stress constitutive equation. However, in the particular case of corotational convective derivative, i.e. $a = 0$, no space derivative appears in the constitutive equation written in the Lagrangian formulation. This means that the nodes move with the characteristics and the equation can be integrated directly along them.

Domain decomposition techniques are finally used to interface the problems in the two regions. In particular, the problem in the wet region is solved using the boundary condition

$$\theta_w(x_i(t), t) = \theta_{\text{guess}} , \quad (5.2)$$

and the problem in the dry region using the boundary condition

$$\frac{\partial \theta_d}{\partial \xi}(x_i(t), t) = \theta'_{\text{guess}} . \quad (5.3)$$

After the very first steps in which θ_{guess} and θ'_{guess} are actually guessed, then θ_{guess} and θ'_{guess} are obtained iteratively weighting the value previously used with the one obtained by the integration of the problem in the other domain, namely

$$\theta_{\text{guess}}^{(i+1)} = \alpha \theta_{\text{guess}}^{(i)} + (1 - \alpha) \theta_d^{(i)} \quad (5.4)$$

$$\theta'_{\text{guess}}^{(i+1)} = \alpha \theta'_{\text{guess}}^{(i)} + (1 - \alpha) \frac{k_m^{(i)}}{k_s^{(i)}} \frac{\partial \theta_w}{\partial \xi} \quad (5.5)$$

where (i) stands for the i -th iteration and α is a relaxation parameter.

The integration is then iterated to convergence, until the temperature and the heat flux conditions (4.20), (4.24) are satisfied within a given accuracy. Because of the smallness of the conductivity of the glass fibers we shall consider in our simulations, the coupled problem is advection dominated, and therefore a couple of iteration is usually sufficient.

The domain decomposition technique can also result helpful in evaluating the nonlinear coefficients appearing in the model, since the result obtained at the previous iteration can be used.

The accuracy of the numerical method is also controlled during integration by computing the total mass of the solid preform

$$M = \int_{x_f(t)}^{x_i(t)} \rho_s \phi_s(x, t) dx + \rho_s \Psi(t) [L - x_i(t)] , \quad (5.6)$$

which must be preserved, of course.

The simulations presented in this section refer to the infiltration of a thermosetting resin in a network of glass fibers. It uses the values of the parameters given in Young et al. (1991) and reported in the Table below for sake of completeness.

Variable	Value	see Equations
ρ_s	2560 Kg/m^3	(2.4), (2.17)
ρ_ℓ	1100 Kg/m^3	(2.4), (2.17)
\tilde{C}_s	670 J/Kg	(2.17)
\tilde{C}_ℓ	1680 J/Kg	(2.22)
k_s	0.168 W/m^0K	(2.27)
k_ℓ	0.0335 W/m^0K	(2.27)
H_c	$1.54 \cdot 10^8 J/m^3$	(2.22)
c_1	$3.7833 \cdot 10^5 sec^{-1}$	(2.30)
c_2	$6.7833 \cdot 10^5 sec^{-1}$	(2.30)
E_1	54418 $J/mole$	(2.30)
E_2	50232 $J/mole$	(2.30)
m_c	0.3	(2.30)
n_c	1.7	(2.30)
δ_g	0.1	(2.29)
$\tilde{\mu}$	$2.78 \cdot 10^{-4} Pa s$	(2.29)
E_μ	18000 $J/mole$	(2.29)
c_μ	1.5	(2.29)
d_μ	1	(2.29)
n_i	25	(2.28)

In addition, according to the data obtained by Kim et al. (1991) and Sommer and Mortensen (1996), the deformability of the solid constituent is reflected in the following stress-volume ratio and permeability-volume ratio relations

$$\begin{aligned} \Sigma_s &= 0.3(e^{25\phi_s} - e^{25\phi_r}) \text{ Pa} , \\ \Sigma &= 0.09(e^{26.4\phi_s} - e^{26.4\phi_r}) \text{ Pa} , \\ K &= 4.95 \cdot 10^{-9} e^{-16(\phi_s - \phi_r)} \text{ m}^2 , \end{aligned} \quad (5.7)$$

where $\phi_r = 0.5$ is the undeformed volume ratio. The behavior of Σ_s and Σ is given in Fig. 3. Finally, we will set the preform length to be $L = 0.3$ m , $\delta_{in} = 0$, and the resin, mold and air temperature to be $300^\circ K$.

In the first set of simulations the infiltration process is driven by a constant inlet pressure of 0.1 MPa. Figure 5 shows the evolution of ϕ_s without curing and in isothermal conditions for $\Lambda = 1$ sec and $\lambda = 0.5$ sec. As already mentioned in Section 3, the elasticity assumption of the dry preform gives rise to a sudden compression of the porous material to a volume ratio $\Psi = 0.5323$ corresponding to the applied inlet pressure. As ΔP is constant (see Eq.(3.19).) the volume ratio in the dry region is constantly held throughout the evolution.

Consequently, the border of the preform suddenly moves to $x_f(t = 0^+) = 1.82$ cm. This means that in response to the applied pressure the preform compresses to $\Psi_0/\Sigma_s^{-1}(\Delta P) = 94.1\%$ of its original length.

As time becomes larger than the relaxation and the retardation time the volume ratio, which according to (4.23) is continuous across $x_i(t)$, presents an overshooting. There is, in fact, a tendency to approach the solution of the case in which both the wet and the dry material behave elastically, but with different stress-volume ratio relations, as in (5.7) (see Farina and Preziosi (1999).) In fact, as already stated, this difference gives rise to a discontinuity of the volume ratio across the infiltration front, since different compressions in the two regions yield the same stress (see also Fig. 4). As there is no curing, the infiltration process is completed in 7.12 sec.

Figure 6a shows the evolution of ϕ_s for the same set of parameters of Fig. 5 but in the non isothermal case with curing. At early times the behavior of the solution is similar to that in Fig. 5. However, after a couple of seconds the effect of polymerization starts affecting infiltration, so that after about 8 seconds, infiltration stops because the resin is gelling near the wetting front. This is then a case in which the driving pressure is not sufficient to fill the preform before the conversion of the resin to a gel. However, as shown in Fig. 6b which refers to δ_c , in the region near the preform border the resin degree of conversion remains for some time below the gel value $\delta_g = 0.1$, but infiltration is blocked by the gelled resin ahead. Therefore, in this region the preform can expand back a little. After about 13 seconds all the resin has gelled and also this backward expansion stops. However the resin cures on, generating heat in the wet region (see Fig. 6b,c), which in turn favours conversion. The chemical reaction is completed after about 50 seconds.

As far as the temperature evolution is concerned, one can notice that the position of the maximum temperature gradually moves from the center of the infiltrated region toward the border $x_f(t)$ of the preform and that the maximum temperature increase is about $45^\circ K$. Due to the smallness of the heat conductivity of glass fibers, heat is more convected by the moving infiltrating resin, than conducted. In this simulation the diffusing effect can be noticed at times much larger than the time taken by the resin to gel, say $t > 30$ sec.

In this case, one can then identify an initial mechanics dominated period (say, up to 5 seconds), an intermediate period (say, from 5 to 12 seconds) in which there is a strong relation between curing and mechanics, another intermediate period (say, from 12 to 40 seconds) dominated by the curing cycle without motion and a final period (say, from 40 seconds on) dominated by heat diffusion. Of course, all aspects are strongly interconnected, periods overlap, and the identification is rather rough. However, the distinction of an infiltration period and a temperature cycle, which is often used in describing some composite manufacturing processes, is not possible in other cases, e.g. in metal matrix composites and if fast reacting resins are used.

The evolution of the infiltration fronts (lines with positive slope) and of the preform borders (lines with negative slope) for different inlet pressures and curing conditions is given in Fig. 7. Figure 7a shows $x_i(t)$ and $x_f(t)$ for the data used in Fig. 6. From this figure it appears that at

early times the infiltration front seems to go like the square root of time. This property of the solution has been proved to be true in the elastic case and if the viscosity were constant by Billi and Farina (2000). In order to put in evidence to which extension this property can be applied also in the non-isothermal case and for different constitutive equations, Fig. 7b plots x_i and x_f versus \sqrt{t} .

As a matter of fact, the dotted line which refers to the data of Fig. 5 (no curing) is undoubtedly a straight line. The full lines which refer to Fig. 6, is very close to a straight line for the first couple of seconds, i.e. when the evolution is mechanics dominated. However, as viscosity strongly depends both on temperature and on the degree of conversion it departs from it when curing becomes important and eventually stops, e.g. if $\Delta P = 0.1$ MPa $x_i(t)$ assumes the constant value 25.4 cm. The dashed lines refer to a inlet pressure $\Delta P = 1$ MPa, which will be discussed at the end of this section.

In Fig. 8 we present the evolution of the volume ratio versus space and time for different relaxation and retardation times. In particular, with respect to Fig. 6, in (a) Λ is ten times larger, while λ is kept of the same order of magnitude and in (b) Λ is two hundred times larger, and λ a hundred times larger to get values closer to those estimated for composite constituents (see Nam et al. (1995).) It can be seen that the evolution is very sensitive to the viscoelastic characteristics of the mixture. In particular, with respect to Fig. 6 a smaller overshooting or no overshooting at all characterizes the solution. This difference is related to the higher value of the retardation time Λ . The instant in which flow stops and, more in general, the curve on the surface characterized by $\delta_c(x(t), t) = \delta_g$ are here more evident. However, it can also be noticed that on the contrary of the deformation and stress states the instant at which infiltration stops depends only weakly on the viscoelastic characteristics of the mixture (e.g., 25.6 cm for $\Lambda = 1$ sec and $\lambda = 0.5$ sec and 25 cm for $\Lambda = 200$ sec and $\lambda = 50$ sec). The evolution of δ_c and θ is in these cases similar to that presented in Fig. 6b,c.

Finally, in Fig. 9 we present the evolution of the volume ratio at a much higher infiltration pressure (1 MPa). This compresses more the preform yielding $x_f(t = 0^+) = 5.26$ cm and a relative initial compression to 82.8% of the original length. However, in this case the infiltration pressure is sufficient to fill the preform in 1.18 seconds for $\Lambda = 1$ sec and $\lambda = 0.5$ sec and in 1.35 seconds for $\Lambda = 200$ sec and $\lambda = 50$ sec. Actually, the infiltration time is so short that the resin has not reacted much ($\max \delta_c = \delta_c(x = L) = 0.008$) yielding a maximum temperature increase of 0.3°K. Also in this case from Fig. 7b (shortest lines) one can appreciate the proportionality of the positions of the infiltration front and of the preform border with the square root of time. In fact, the flow is so fast that infiltration is achieved before enough curing can take place.

6. Conclusions

We have presented a new model conceived to simulate some non-isothermal infiltration problems occurring when fabricating composites by infiltration processes, though the model can also be applied with the obvious changes to compression and autoclave moulding processes, and to

other industrial processes involving infiltration in deformable porous materials, e.g. sponge-like materials.

The solid preform is not assumed rigid, and therefore it can deform during the application of the pressure and temperature cycle. In addition, while infiltrating the resin undergoes an exothermic crosslinking chemical reaction, and may gel before infiltration is complete, stopping the infiltration.

The problem presents the formation of three time-dependent domains, the first one occupied by the liquid only, the second one by the solid preform wet by the curing resin, and the third one consisting of the uninfiltreated solid preform.

In the one-dimensional case, the solution in the first domain is trivial, and the mechanical problem in the third domain can be reduced to the integration of an ordinary differential equation determining either the location of the infiltration front or the volume ratio in the dry region, depending on whether the parameter which is controlled to drive infiltration is the inflow velocity or the inlet pressure. In this last case it is shown, among other things that the preform initially compresses to Ψ_0/Ψ_P of its initial length where Ψ_0 is the initial volume ratio of the preform and Ψ_P is the one yielding a stress in the dry preform equal to the inlet pressure. This effect can be reduced by pre-compressing, if possible, the preform with a mold pressure equal to the infiltration pressure.

The simulations presented show how the model can be used to determine the evolution of the deformation state and the parameter range for which the preform is completely infiltrated before resin gels.

They also show that when more precise measurements on the mechanical properties of the materials used are available, the model can help identifying and optimizing the production cycle to be used in practice.

However, before the three-dimensional model presented here can be operatively applied, some problems related to the determination of the interface conditions, to the difference between volume fraction and surface area fraction in anisotropic materials and to the identification of the constitutive equations must be addressed and need a careful study. When this is done, the simulation of processes presenting racetracking and non-homogeneous and anisotropic permeabilities can be addressed.

Acknowledgements. The authors are grateful to the Italian Ministry for the University and Scientific Research (M.U.R.S.T.) and to the National Research Council (C.N.R. Contract 96.03858.CT01 on Multicomponent Flows) for funding the present research.

References

Ambrosi, D. & Preziosi, L. 1998 Modelling matrix injection in initially dry and deformable

- preforms. *Composites A*, **29**, 5–18.
- Ambrosi, D. & Preziosi, L. 2000 Modelling injection moulding processes with deformable porous preforms. *SIAM J. Ind. Appl. Math.* In press.
- Antonelli, D. & Farina, A. 1999 Resin transfer moulding: Mathematical modelling and numerical simulations, *Composites A*, 1367–1385.
- Bellomo, N. & Preziosi, L. 1995 *Modelling, Mathematical Methods and Scientific Computation*. CRC Press.
- Billi, L. & Farina, A. 2000 Unidirectional infiltration in deformable porous media: Mathematical modeling and self similar solution. *Quart. Appl. Math.* In press.
- Bowen, R.M. 1980 Incompressible porous media models by use of the theory of mixtures. *Int. J. Engng. Sci.* **18**, 1129–1148.
- Chan, A.W. & Hwang, S.T. 1991 Modeling the impregnation process during resin transfer molding. *Polymer Engng. Sci.* **31**, 1149–1156.
- Chan, A.W. & Hwang, S.T. 1992 Modeling nonisothermal impregnation of fibrous media with reactive polymer resin. *Polymer Engng. Sci.* **32**, 1310–318.
- Chan, A.W. & Hwang, S.T. 1993 Modeling resin transfer molding of polyimide (PMR-15)/fiber composites *Polymer Compos.* **14**, 524–528.
- Clyne, T.W. & Mason, J.F. 1987 The squeeze infiltration process for fabrication of metal-matrix composites. *Metall. Trans. A* **18A**, 1519–1530.
- de Boer, R. 1996 Highlights in the historical development of the porous media theory: Toward a consistent macroscopic theory, *Appl. Mech. Rev.*, **49**, 201–262.
- Farina, A. & Preziosi, L. 1999 Free boundary problems in the production of composites. Proceedings of the Conference *Free Boundary Problems*, Heraklion, Crete. In press.
- Gonzalez-Romero, V.M. & Macosko, C.W. 1990 Process parameters estimation for structural reaction injection molding and resin transfer molding. *Polym. Engng. Sci.* **30**, 142–146.
- Gutowski, T.G. 1985 A resin flow/fiber deformation model for composites. *SAMPE Quart.*, **16**, 58–64.
- Han, K., Trevino, L., Lee, L.J. & Liou, M.J. 1993 Fiber mat deformation in liquid composite molding. I: Experimental analysis. *Polymer Compos.* **14**, 144–150.
- Han, K., Lee, L.J. & Liou, M.J. 1993 Fiber mat deformation in liquid composite molding. II: Modeling. *Polymer Compos.* **14**, 151–160.
- Joseph, D.D. 1990 *Fluid Dynamics of Viscoelastic Liquids*, Springer-Verlag.
- Kamal, M.R. & Sourour, S. 1973 Kinetics and thermal characterization of thermoset cure. *Polymer Engng. Sci.* **13**, 59–64.
- Kim, Y.R., McCarthy, S.P. & Fanucci, J.P. 1991 Compressibility and relaxation of fiber reinforcements during composite processing. *Polymer Compos.* **12**, 13–19.
- Lacoste, E., Aboufatah, M., Danis, M. & Girot, F. 1993 Numerical simulation of the infiltration

- of fibrous preforms by a pure metal. *Metall. Trans. A* **24A**, 2667–2678.
- Lacoste, E., Danis, M., Girod, F. & Quennisset, J.M. 1991 Numerical simulation of the injection moulding of thin parts by liquid metal infiltration of fibrous preform. *Mater. Sci. Engng. A* **A135**, 45–49.
- Lekakou, C., Johari, M.A.K.B. & Bader, M.G. 1996 Compressibility and flow permeability of two dimensional woven reinforcements in the processing of composites, *Polymer Compos.* **17**, 666–672.
- Liu, I.S. 1980 On chemical potential and incompressible porous media. *J. Mécanique* **19**, 327–342.
- Lin, R.J., Lee, L.J. & Liou, M.J. 1991 Non-isothermal mold filling and curing simulation in thin cavities with preplaced fiber mats. *Intern. Polymer Processing* **6**, 356–369.
- Lin, R.J., Lee, L.J. & Liou, M.J. 1993 Mold filling and curing analysis in liquid composite molding. *Polymer Compos.* **14**, 71–81.
- Malvern, L.E. 1969 **Introduction to the Mechanics of a Continuous Medium**, Prentice-Hall.
- Markov, K. & Preziosi, L. 1999 **Heterogeneous Media: Micromechanics, Modelling, Methods and Simulations**, Birkhäuser.
- Mortensen, A. & Wong, T. 1990 Infiltration of fibrous preforms by a pure metal: Part III. Capillary phenomena. *Metall. Trans. A* **21A**, 2257–2263.
- Müller, I. 1975 Thermodynamics of mixtures of fluids. *J. Mécanique* **14**, 267–303.
- Nam, J.D., Seferis, J.C., Kim, S.W. & Lee, K.J. 1995 Gas permeation and viscoelastic deformation of prepregs in composite manufacturing processes. *Polymer Compos.* **16**, 370–377.
- Parker, K.H., Mehta, R.V. & Caro, C.G. 1987 Steady flow in porous, elastically deformable materials. *J. Appl. Mech.* **54**, 794–800.
- Preziosi, L. 1996 The theory of deformable porous media and its application to composite material manufacturing. *Surveys in Mathematics for Industry* **6**, 167–214.
- Preziosi, L., Joseph, D.D. & Beavers, G.S. 1996 Infiltration in initially dry, deformable porous media. *Int. J. Multiphase Flows* **22**, 1205–1222.
- Rajagopal, K.R. & Tao, L. 1995 *Mechanics of Mixtures*. World Scientific.
- Reboredo, M.M. & Rojas, A.J. 1988 Molding by reactive injection of reinforced plastics. *Polymer Engng. Sci.* **28**, 485–490.
- Rudd, C.D. & Kendall, K.N. 1992 Towards a manufacturing technology for high-volume production of composite components. *Proc. Instn. Mech. Engrs.* **206**, 77–91.
- Rudd, C.D., Owen, M.J. & Middleton, V. 1990 Effects of process variables on cycle time during resin transfer moulding for high volume manufacture. *Mater. Sci. Techn.* **6**, 656–665.
- Sommer, J.L. & Mortensen, A. 1996 Forced unidirectional infiltration of deformable porous media, *J. Fluid Mech.* **311** 193–215.

Terzaghi, K. 1923 Die berechnung der durchlässigkeitsziffer des tones aus dem verlauf der hydrodynamischen spannungserscheinungen (A method of calculating the coefficient of permeability of clay from the variation of hydrodynamic stress with time), *Sitznughrichte Akad. Wissen. Wien of Mathem. Naturw. Kl. IIa* **132**, 125–138.

Trevino, L., Rupel, K., Young, W.B., Liou, M.J. & Lee, L.J. 1991 Analysis of resin injection molding in molds with preplaced fiber mats. I: Permeability and compressibility measurements. *Polymer Compos.* **12**, 20–29.

Yamauchi, T. & Nishida, Y. 1995 Infiltration kinetics of fibrous preforms by aluminum with solidification. *Acta Metall. Mater.* **43**, 1313–1321.

Young, W.B., Rupel, K., Han, K., Lee, L.J. & Liou, M.J. 1991 Analysis of resin injection molding in molds with preplaced fiber mats. II: Numerical simulation and experiments of mold filling. *Polymer Compos.* **12**, 30–38.

Young, W.B. & Chiu, C.W. 1995 Study of compression transfer molding. *J. Compos. Mater.* **29**, 2180–2191.

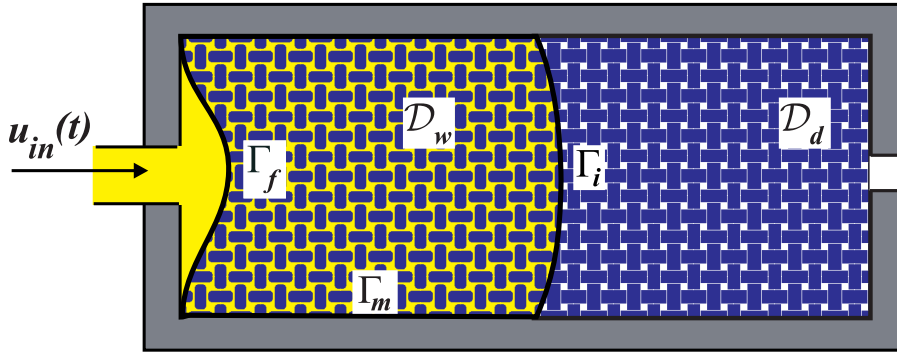


Figure 1 — Geometrical description of the infiltration problem.

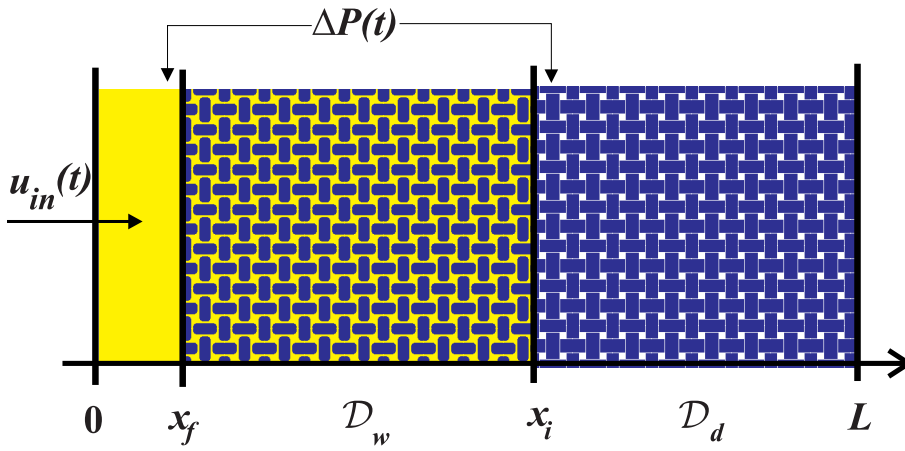


Figure 2 — Schematization of the one-dimensional infiltration problem.

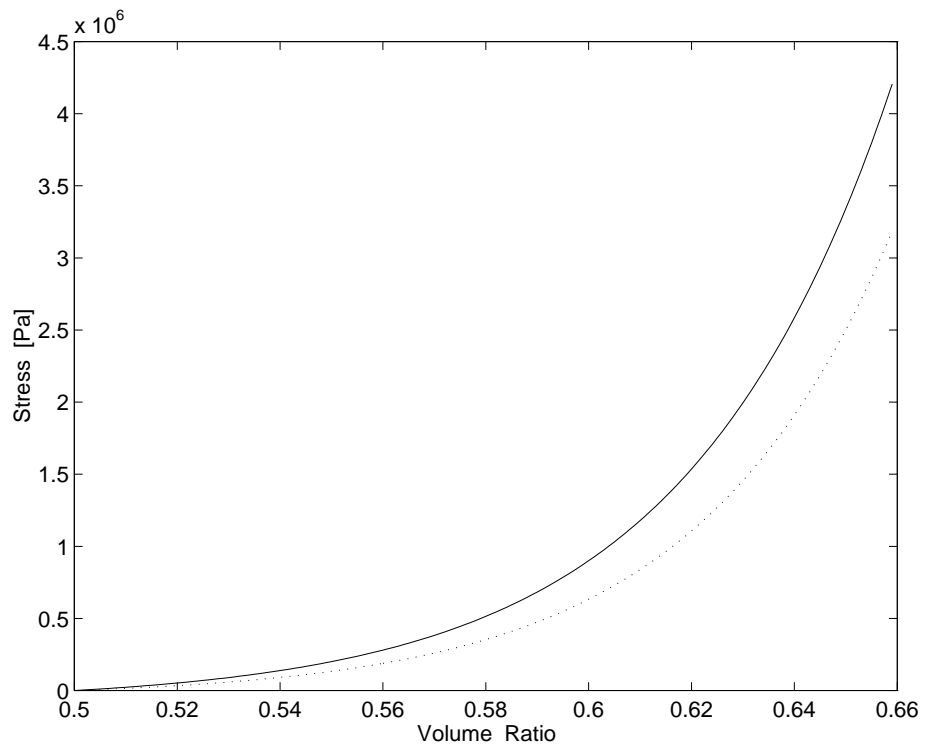


Figure 3 — Stress-volume ratio relation for the wet (dotted line) and the dry preform (full line).

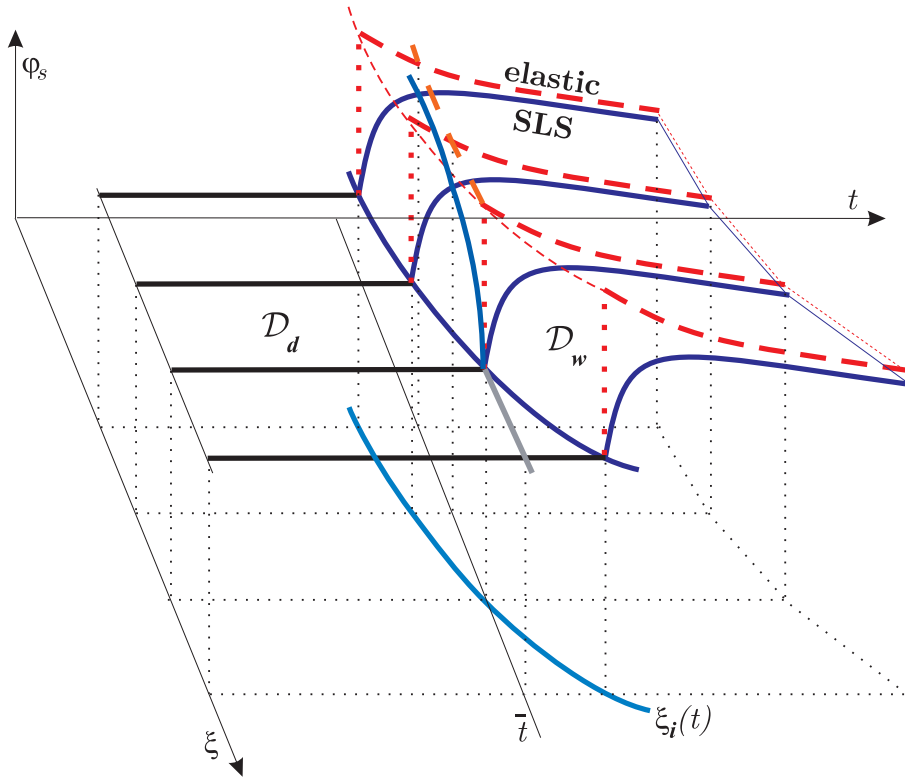


Figure 4 — Difference between elastic response and the standard linear solid response at the passage of the infiltration front. ξ is the Lagrangian coordinate labelling a solid particle. ξ_i is the infiltration front. In the elastic case (heavy dashed lines) when the dry particle is wet by the infiltration front (follow the arrowed line), the volume around it suddenly expands because of stress continuity and of the fact that $\Sigma(\phi) < \Sigma_s(\phi)$. In the standard linear solid case (heavy full lines) the same volume takes some time to adjust and, therefore, the surface $\phi_s(\xi, t)$ is continuous during infiltration. At a certain time \bar{t} the solution will have the qualitative behavior shown by the corresponding curve.

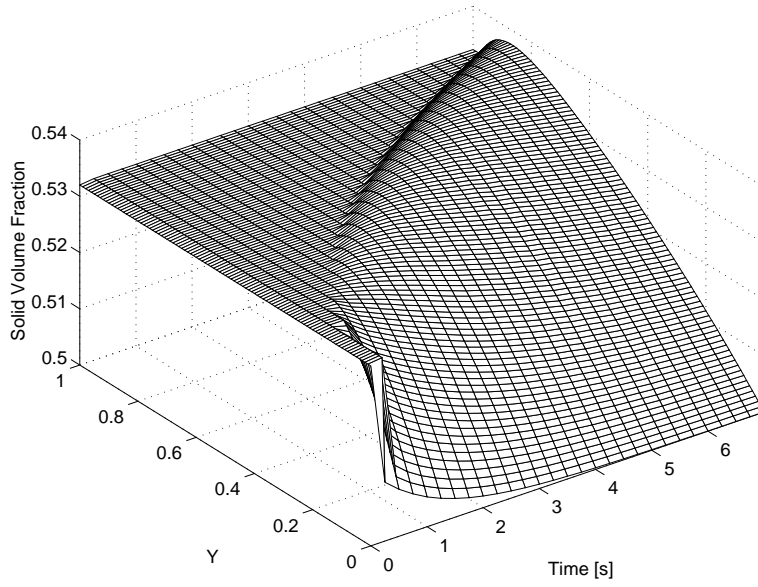
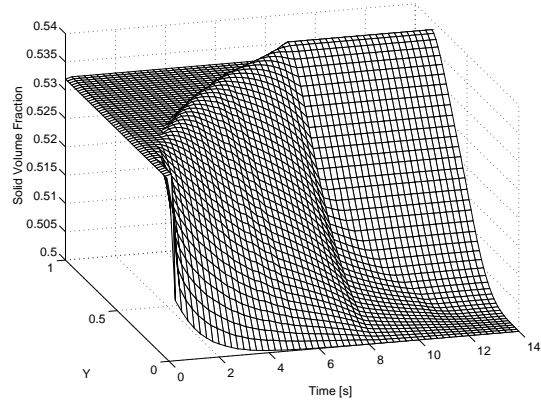
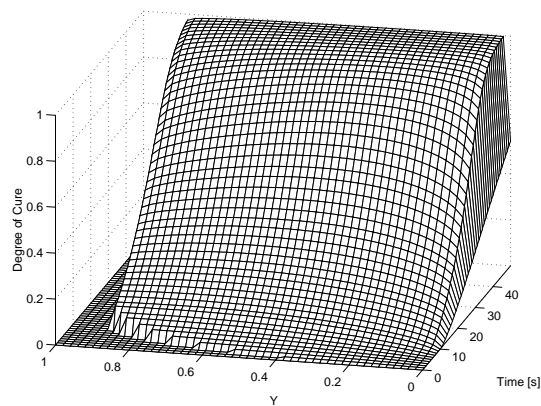


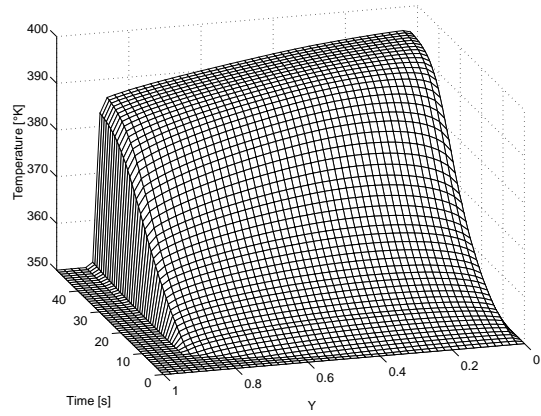
Figure 5 — Infiltration due to a constant pressure drop $\Delta P = 0.1 \text{ MPa}$ for $\Lambda = 1 \text{ sec}$ and $\lambda = 0.5 \text{ sec}$ without curing. The normalized coordinate is $Y = (\xi - \xi_f(0^+))/(L - \xi_f(0^+))$ where $\xi_f(0^+) = 1.82 \text{ cm}$.



(a)

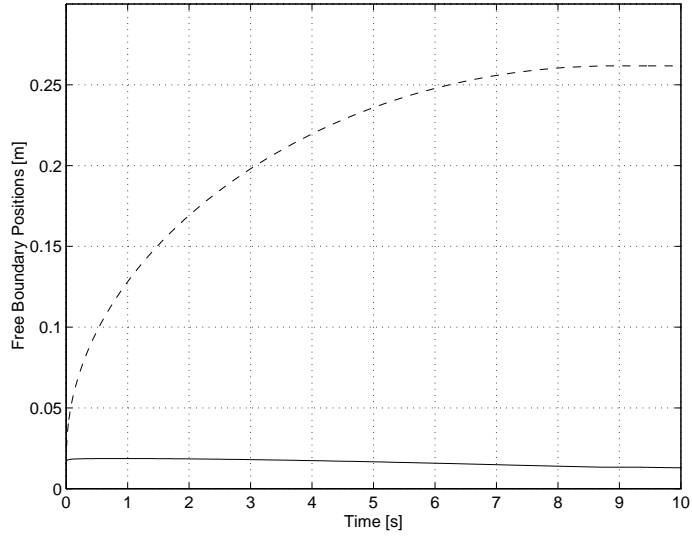


(b)

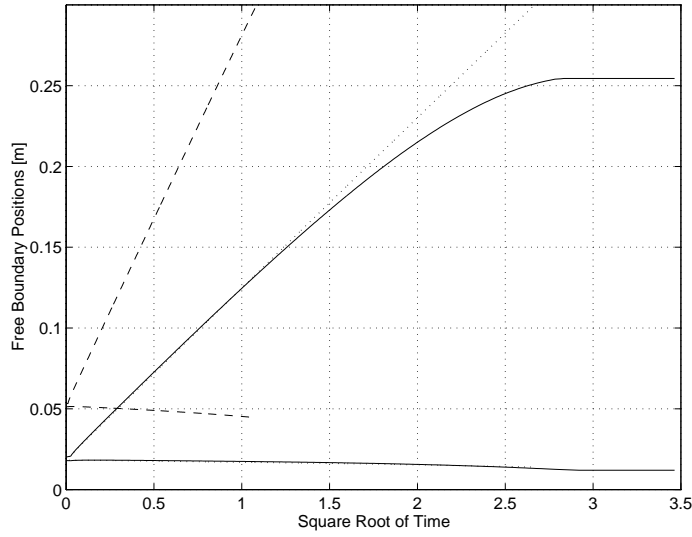


(c)

Figure 6 — Infiltration due to a constant pressure drop $\Delta P = 0.1 \text{ MPa}$ for $\Lambda = 1 \text{ sec}$ and $\lambda = 0.5 \text{ sec}$. The normalized coordinate is $Y = (\xi - \xi_f(0^+)) / (L - \xi_f(0^+))$ where $\xi_f(0^+) = 1.82 \text{ cm}$. (a) Volume ratio. (b) Degree of cure. (c) Temperature. After about 8 seconds infiltration stops and the solid volume ratio near the infiltration front does not change in time.

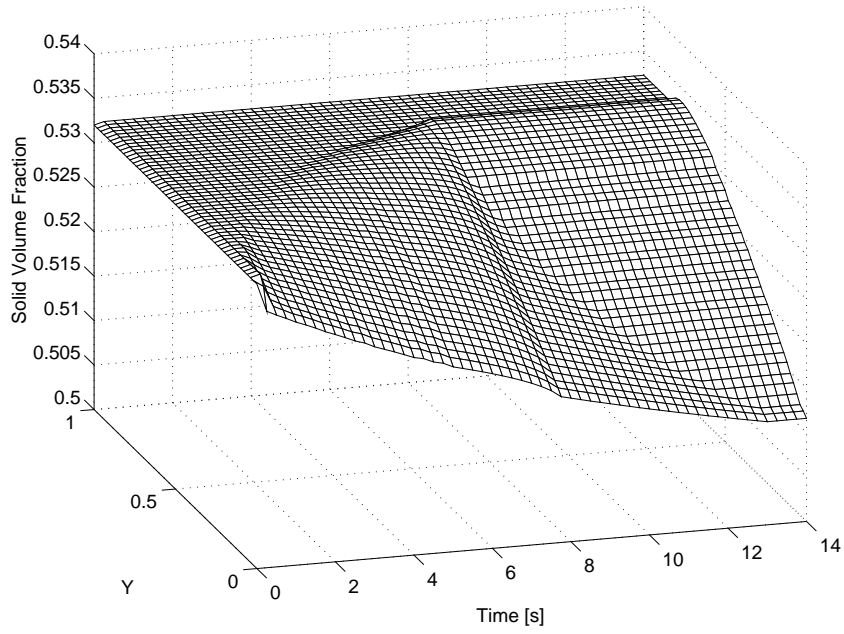


(a)

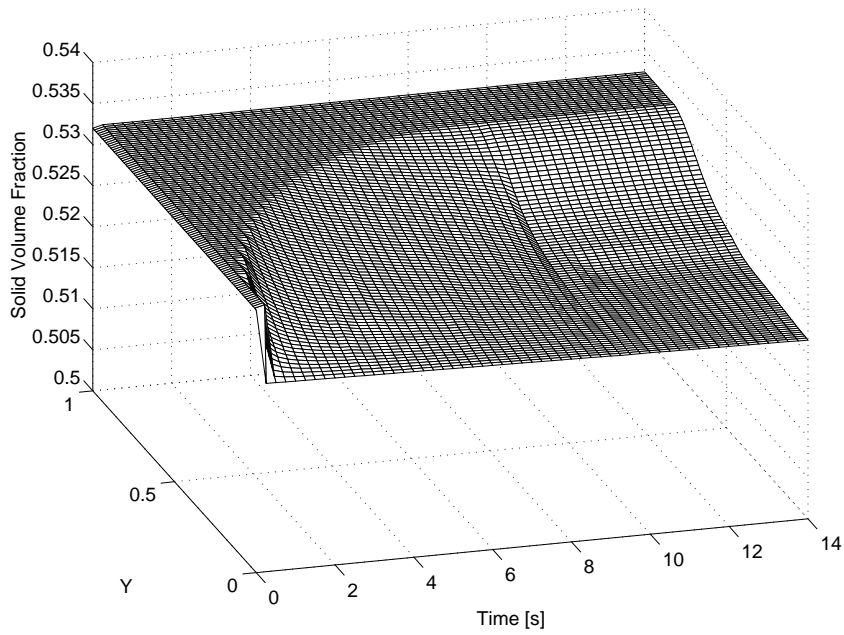


(b)

Figure 7 — Temporal evolution of the position of the infiltration front and of the preform border for $\Lambda = 1$ sec, $\lambda = 0.5$ sec. In (a) $\Delta P = 0.1$ MPa. At $t \approx 8$ sec infiltration stops and the dashed line becomes constant. In (b) the interface positions is plotted versus \sqrt{t} for different flow conditions: dotted lines refer to the case without curing, full lines to $\Delta P = 0.1$ MPa with curing and dashed lines to $\Delta P = 1$ MPa with curing.

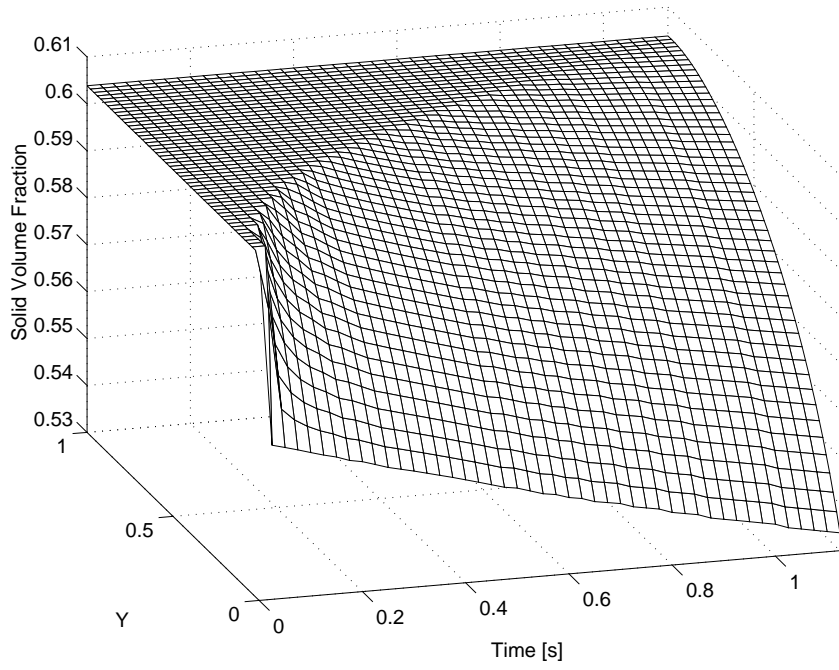


(a)

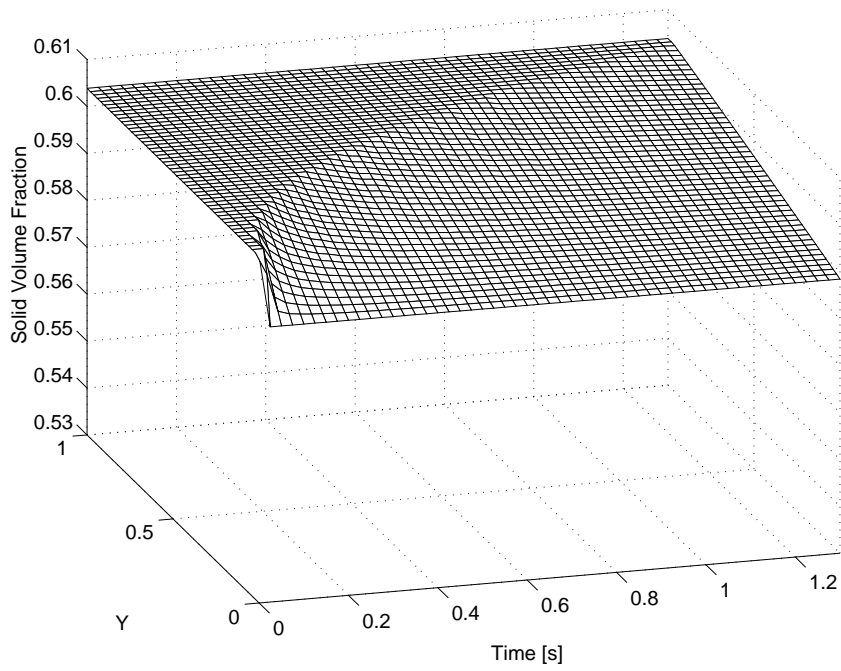


(b)

Figure 8 — Evolution of the volume ratio for $\Delta P = 0.1$ MPa and (a) $\Lambda = 10$ sec, $\lambda = 1$ sec. (b) $\Lambda = 200$ sec, $\lambda = 50$ sec. The normalized coordinate is $Y = (\xi - \xi_f(0^+))/(L - \xi_f(0^+))$ where $\xi_f(0^+) = 1.82$ cm.



(a)



(b)

Figure 9 — Evolution of the volume ratio for $\Delta P = 1$ MPa and (a) $\Lambda = 1$ sec, $\lambda = 0.5$ sec. (b) $\Lambda = 200$ sec, $\lambda = 50$ sec. The normalized coordinate is $Y = (\xi - \xi_f(0^+))/(L - \xi_f(0^+))$ where $\xi_f(0^+) = 5.26$ cm.